Adsorption of alkali adatoms on graphene supported by the Au/Ni(111) surface

C. S. Praveen, Simone Piccinin, and Stefano Fabris[*]

CNR-IOM DEMOCRITOS, Istituto Officina dei Materiali, Consiglio Nazionale delle Ricerche and SISSA,
Via Bonomea 265, 34136 Trieste, Italy

We study alkali-metal adsorption on supported graphene by means of density-functional-theory calculations that include dispersion corrections. Graphene supported by the Au/Ni(111) surface is an important system for fundamental studies because this surface allows one to support graphene, preserving the electronic properties of freestanding graphene. We investigate the binding energetics as well as the structural and electronic properties of Li, Na, K, and Rb atoms adsorbed or intercalated at the graphene/Au/Ni(111) interfaces and compare the results to those obtained on freestanding graphene. Both the adsorption and intercalation of the alkali atoms induce electron doping to the graphene π bands that display a quasirigid-energy shift. Electron doping by alkali atoms preserves the Dirac cone of graphene, which shifts downwards due to the negative polarity of the doping. The metallic or ionic character of the alkali dopant is controlled by its position relative to graphene. All of the investigated alkali atoms display an energetic preference to intercalate between graphene and the Au/Ni support. These results shed light on the relationship between graphene electron doping, the alkali-atom adsorption site, and the charge transfers at the graphene/support interface.

I. INTRODUCTION

Research focusing on manipulating graphene so as to exploit its properties in technological applications has been growing since its first successful exfoliation [1]. The distinct electronic, magnetic, and mechanical properties of graphene pave the way to novel devices and applications. Many of these interesting properties of freestanding graphene arise from characteristic features in the band structure, namely the Dirac cone formed at the Fermi level from the intersection of the π and $\pi^\star$ C states [2]. However, in the case of supported, doped, or functionalized graphene, the interaction with the support, adsorbed dopants, or functional groups may significantly alter its characteristic band structure and hence the physical and chemical properties. It is therefore important to provide a fundamental understanding of the effects of substrates or surface dopants on the electronic properties of graphene.

Transition-metal substrates have been extensively studied as graphene supports and can be classified according to the interaction strength in two groups. When graphene is chemisorbed, e.g., on Co, Ni, Ru, and Pd [3–6], there is a significant overlap between the metal d bands and the graphene π bands. This leads to a strong graphene-support interaction that significantly affects the Dirac-cone feature and opens a gap in the band structure. On the other hand, when graphene is physisorbed on metal substrates such as Ir, Pt, Au, and Cu [3,7–10], the weaker interaction with the substrate typically preserves the Dirac cone. The position of the Fermi level relative to the cone is, however, affected and controlled by interface charge-transfer effects. Among transition metals, Ni(111) has the lowest mismatch with respect to the graphene lattice ($\sim$1.2%). This small mismatch allows for an epitaxial growth of graphene with very few structural defects and without moiré patterns [11]. We note that the actual adsorption

geometry of graphene on the Ni(111) substrate is still being debated [12–14].

Ideally, the perfect 1×1 lattice registry between the C network and the Ni(111) periodicity can enable the manipulation of graphene/Ni(111) interfaces and promote their technological application. However, taking advantage of the electronic properties of graphene requires a substrate that allows for graphene manipulation and preserves the characteristic Dirac cone in the electronic structure. Angle-resolved photoemission spectroscopy (ARPES) measurement [15,16] and electron energy-loss spectroscopy (EELS) [17] have shown that the graphene Dirac cone can be restored by intercalation of noble-metal atoms at the graphene/Ni(111) interface. In particular, one monolayer (ML) of Au at the Ni(111) surface allows for supporting graphene whose electronic structure displays a gapless Dirac cone similar to the one of freestanding ideal graphene. For device applications, the graphene band structure has to be engineered. One way of doing this is chemical doping using alkali atoms. It has been reported [18] that the Fermi level of the graphene/substrate system can be controlled by a proper choice of the alkali atom, thereby opening the possibility of applications in tunable electronic devices.

Another motivation for studying alkali atom adsorption on graphene is superconductivity: Despite the extraordinary properties of graphene, realization of superconductivity in pristine graphene remains challenging. It has been suggested that electron doping should be a possible route to achieve superconductivity via phonon mediation [19]. Electron-phonon coupling-induced superconductivity has been reported in several other carbon-related materials, especially graphite intercalated compounds (GICs) [20–22], fullerene crystals [23,24], and nanotubes [25,26]. Partially occupied dopant-derived bands through incomplete ionization is the key to superconductivity in all of these compounds. The electron-electron interaction inhibiting superconductivity could efficiently be suppressed in supported graphene by the screening from the metal substrate. It has been demonstrated that electron-phonon coupling could be introduced by doping with alkali atoms

_____
[*]fabris@sissa.it

on metal-supported graphene, as in the case of alkali-derived GICs [27].

In summary, a detailed understanding of the electronic structure of alkali-doped metal-supported graphene is instrumental in a wide range of fundamental and applied scientific issues. In the present work, we employ density-functional-theory (DFT) calculations to systematically investigate the effects on the electronic structure of doping-supported graphene with adsorbed and intercalated alkali atoms.

II. METHODS

Spin-polarized density-functional-theory simulations of alkali adsorption on pristine and supported graphene were performed by employing the Pedrew-Burke-Ernzerhof (PBE) exchange and correlation functional [28]. The electron-ion interaction was modeled with ultrasoft pseudopotentials, while the valence electrons were described with a plane-wave basis set limited by a kinetic-energy cutoff of 35 Ry. We used a Γ-centered $8 \times 8 \times 1$ Monkhorst-Pack sampling for the irreducible part of the Brillouin zone and a Gaussian smearing of 0.01 Ry. Dispersion terms were included in the DFT calculations with the Grimme approach (DFT-D) [29]. To visualize the atom-projected band structure, we used the technique of resolving the projected density of states in the k space [30], where the Kohn-Sham states, at every k point, are projected on atomic states. For this purpose we performed non-self-consistent calculations using 200 k points along the Γ'-K'-M'-Γ' path in the irreducible part of the Brillouin zone. All of the calculations used periodic boundary conditions and were performed with the PWscf code included in the QUANTUM ESPRESSO distribution [30].

The pristine Ni(111) surface was modeled with a five-layer supercell slab having an optimized lattice parameter of 2.48 Å. We modeled the graphene/Ni(111) interface with a (2×2) supercell by adopting the so-called top-fcc arrangement of carbon atoms on the Ni(111) surface, containing four Ni surface atoms [11]. The PBE optimized lattice parameter of graphene is 2.46 Å. The very small mismatch (1%) between the two lattices was compensated by stretching the graphene lattice to match the one of the Ni(111) surface. Following recent theoretical models [31], we have simulated a 3/4 ML Au coverage on Ni(111) by including three gold atoms on the top, fcc, and hcp sites of a (2×2) Ni(111) supercell exposing four Ni atoms on the surface. Alkali adsorption was modeled by placing a single alkali atom above or below the hollow site of the honeycomb graphene 2×2 lattice. We employed the same coverage of alkali atoms in all of the calculations, namely, a 1/8 ML corresponding to a 2×2 superlattice. Fixing the same coverage for all alkali atoms allows for direct comparison between the adsorption properties of different adatoms. To optimize the geometry, we fix the Ni atoms at the lowermost two layers of the slab to their bulk positions, while all other atoms are allowed to relax. Along the direction perpendicular to the surface, a minimum of 10 Å vacuum is ensured to avoid the spurious interaction between the periodic images. The top and side views of the structural models that we have employed in the present study are displayed in Fig. 1. All of the binding/intercalation energies (E_b) are calculated in terms
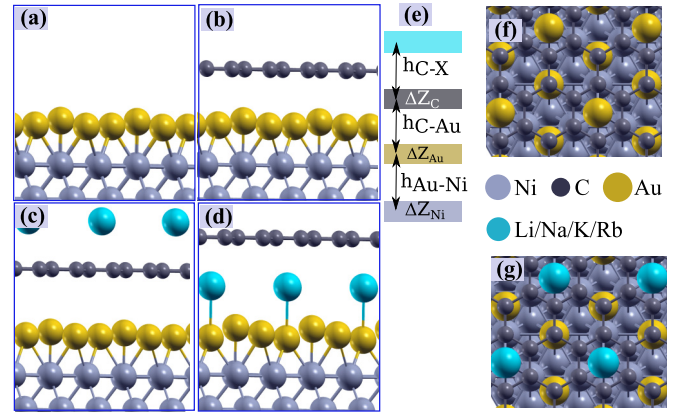
FIG. 1. (Color online) (a) Side and top views of the model Au/Ni(111) surface, (b),(f) graphene/Au/Ni(111) system with (c),(g) adatoms adsorbed and (d) intercalated. (e) The definition of the structural parameters reported in the text: The colored blocks represent the substrate (light gray/yellow), graphene (dark gray), and alkali (light blue) layers.

of the following energy difference:

$$E_b = E_{\text{total}} - (E_{\text{sub}} + E_{\text{alkali}}), \tag{1}$$

where E_{total} and E_{alkali} represents the total energies of the supercells describing the supported alkali adatom and the isolated gas-phase alkali atom, respectively. E_{sub} represents the energy of the supercell describing the support, namely, a freestanding graphene or the graphene/Au/Ni(111) slab. E_{alkali} is the energy of an alkali atom in vacuum, which is calculated by placing a single atom in a cubic supercell having a size of 18.5 Å.

III. RESULTS AND DISCUSSIONS

A. Doping freestanding graphene with alkali atoms

We start from assessing the structure and energetics of the adsorption of alkali atoms on the freestanding graphene. These results are reported in Table I and set the baseline for analyzing the substrate effects that will be presented in the following. The binding energy E_b displays weak variations as a function

TABLE I. Energetics (in eV) of alkali atoms adsorbed on pristine graphene. E_{H-T} is the energy difference between the hollow (H) and top (T) sites for the corresponding atom. E_b is the binding energy of the adatoms on pristine graphene; $E_{\text{coh}}^{2 \times 2}$ is the cohesive energy of the alkali monolayer, calculated as the energy difference between the 2×2 layer of alkali adatoms and an isolated adatom; $E_{\text{coh}}^{\text{bulk}}$ is the bulk cohesive energy of the alkali atom; h_{C-X} is the vertical distance between the graphene plane and the alkali adatom; and ΔE_{free} is the shift in the Dirac cone with respect to the Fermi level.

Alkali	E_{H-T}	E_b (Gr)	$E_{\text{coh}}^{2 \times 2}$	$E_{\text{coh}}^{\text{bulk}}$	h_{C-X}	ΔE_{free}
Li	−0.30	−1.37	0.36	1.63	1.84	−1.48
Na	−0.10	−0.95	0.44	1.11	2.38	−1.06
K	−0.07	−1.15	0.61	0.93	2.76	−1.07
Rb	−0.06	−1.21	0.60	0.86	2.91	−1.05
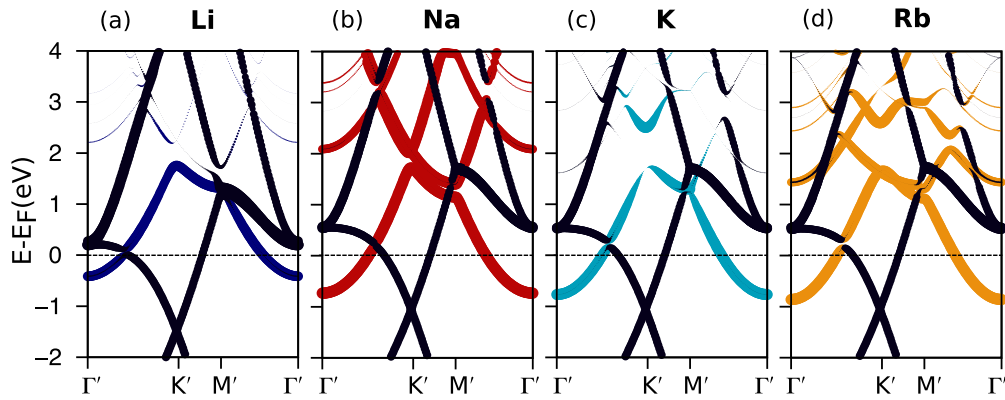
FIG. 2. (Color online) Atom-projected band structure of freestanding graphene with adsorbed alkali atoms. The black line shows the contribution of carbon atoms, while colored lines show the contribution from the alkali adatom. The thickness of the line is proportional to the weight of the alkali-atom projection. The Fermi level is taken as zero and is represented by dotted lines.

of the binding site. Within the approximations used in the present DFT study, alkali-atom adsorption on the bridge and top graphene sites is energetically nearly degenerate, while the hollow site is the most stable. The energy difference between the hollow and top sites is reported in Table I as E_{H-T}. The minimum-energy difference is −0.06 eV, i.e., actually smaller than the error bar of the present calculations. These results are consistent with previous reports [32,33].

All of the adatoms are found to adsorb on freestanding graphene with binding energies ranging from 0.95 to 1.21 eV (energies are calculated for adsorption on the most stable hollow site). Li and Na display the highest and lowest binding energies, respectively. There is no general trend in the adsorption energy of the alkali atoms to graphene, as previously noted [34,35].

The adsorption of alkali atom induces very little distortion in the graphene lattice, which remains almost flat. The optimized height (h_{X-C}) of the alkali adatom from the graphene plane displays a large variation: h_{X-C} monotonically increases from 1.84 Å for Li to 2.91 Å for Rb. Indeed, the optimized height linearly correlates with the adsorbent atomic and ionic sizes. The heights are calculated from the relaxed structure by taking the difference in the average z coordinates of the respective layers.

The adsorption of alkali atoms on pristine graphene induces a charge transfer from the alkali atoms, which become partially ionic, to the graphene plane, which increases the number of electrons in its unoccupied C-π bands. This electron doping of graphene affects the relative position of the Fermi level with respect to the Dirac cone, which shifts to the lower energies (see black lines in the atom-projected band structure in Fig. 2). The energy shifts of the C-π bands and of the Dirac cone with respect to undoped graphene (ΔE_{free}) are reported in Table I and are consistent with previous reports [36].

Li doping in the LiC$_8$ stoichiometry induces an energy shift of 1.5 eV, while all other alkali atoms induce smaller energy shifts of ≈1.0 eV. This qualitative difference is further supported by Bader charge analysis [37]. Li transfers ≈0.7e to the graphene plane, while all other atoms transfer roughly 0.4e of charge.

The atom-projected band structure analysis displayed in Fig. 2 clearly shows that adsorption of the alkali atoms at this

high coverage preserves the metallic bands of the alkali-atom overlayer. The Fermi level crosses the band formed by the s states of the dopant atom (see color lines in Fig. 2). This suggests that despite the charge transfer to graphene, a considerable metallic bonding persists between the alkali atoms in the 2 × 2 planar arrangement. Indeed, the cohesive energy of this planar structure, calculated as the total-energy difference between the 2 × 2 alkali-atom unsupported layer and that of an isolated alkali atom ($E_{\text{coh}}^{2\times2}$) is a considerable fraction of the bulk cohesive energy ($E_{\text{coh}}^{\text{bulk}}$) of the corresponding alkali metal (see Table I). For the case of Li, the cohesive energies of the 2 × 2 layer and bulk systems are 0.36 and 1.63 eV/atom, respectively. The cohesive energies of the overlayer increases going down the group from 0.36 to 0.60 eV/atom, while the cohesive energy of the bulk systems decreases going down the period, from 1.63 to 0.86 eV/atom for Li and Rb, respectively. The cohesive energy of the 2 × 2 overlayer varies therefore from 22% to 69% of the bulk cohesive energy. It is evident that at these coverages, the metallic character of the alkali-atom overlayer plays an important role into its stability.

B. Substrate effects on graphene electronic properties

Before studying the adsorption of alkali atoms on supported graphene, we clarify the effects on the graphene electronic structure due to the interaction with the metallic substrate, emphasizing the importance of including dispersion terms in the DFT calculations.

Despite a reasonable description of ionic and covalent bonds, local density approximation (LDA) and generalized gradient approximation (GGA) functionals fail to give a satisfactory description of nonlocal dispersive forces. Therefore, a better description of the van der Waals forces is necessary when they play a significant role in binding, as in the present case. It has been shown [38] that GGA gives a poor description of graphene/Ni interfaces and that LDA, due to a fortuitous error cancellation, succeeds in giving reasonable energetics [38,39]. In fact, using a GGA functional while neglecting dispersion corrections results in no binding of graphene to the Ni substrate [40]. We therefore employ the Grimme approach [29] to include dispersion interaction in our GGA calculations. In the Grimme approach, van der Waals interactions are tackled
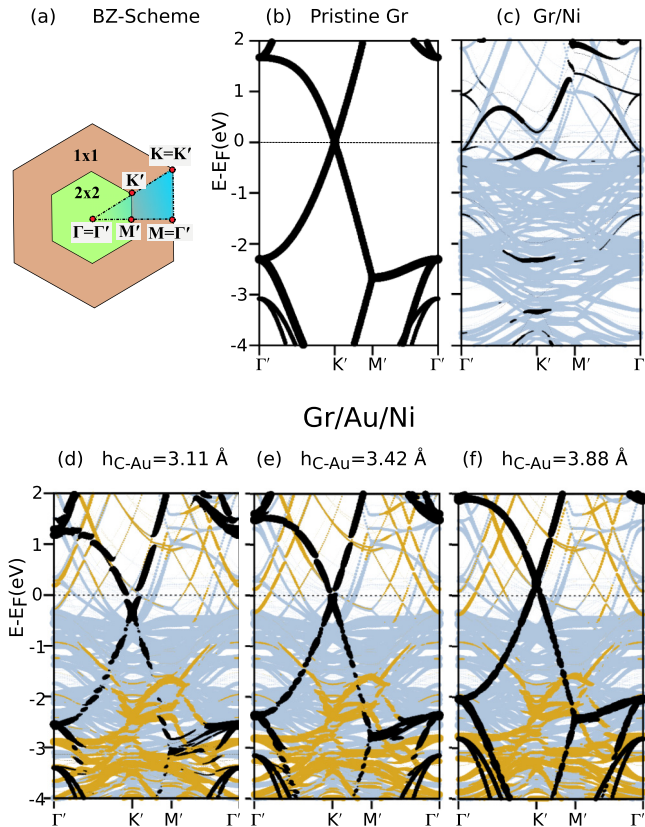
FIG. 3. (Color online) (a) Brillouin zones of graphene represented with 2×2 and 1×1 supercells. Atom-projected band structure of (b) pristine graphene, (c) graphene on Ni(111), and (d) graphene on Au/Ni(111). (e),(f) The atom-projected band structure calculated by artificially increasing the separation between graphene and Au to 3.42 and 3.88 Å, respectively. Black, light blue, and gold colors represent carbon-, Ni-, and Au-derived bands, respectively. Zero is taken as the Fermi level and is represented by dashed lines.

by adding a semiempirical term (E_{disp}) to the bare Kohn-Sham energy. E_{disp} contains the pairwise dispersion coefficient C_6 as well as the cutoff radius as empirical parameters. DFT-D is robust and computationally inexpensive. However, the parameters used are system independent and do not affect the electronic structure. Recent efforts to go beyond the present approach includes Grimme's DFT-D3, wherein the dispersion coefficients C_6 are geometry dependent, as they are adjusted on the basis of local geometry (coordination number) around the interacting pair of atoms. A different approach is the vdW-DF and its second generation vdw-DF2 functionals [41,42]. The approach remains sophisticated due to the necessity to evaluate multidimensional integrals. For a comprehensive review of several dispersion correction methods, we refer to Ramalho *et al.* [43].

First of all, we assess how the substrate affects the electronic properties of pristine graphene, as a reference for the doping of supported graphene. We plot in Fig. 3 the atom-projected band structure of pristine and supported graphene. All of these calculations are performed in 2×2 supercells, whose Brillouin zone (BZ) is folded with respect to the corresponding one of the primitive graphene cell. For clarity, a scheme relating

the sizes and high-symmetry points in the BZs of the primitive and 2×2 supercells is included in Fig. 3(a).

In Fig. 3(b), the Dirac point of the pristine graphene is clearly visible at the Fermi level, as expected, with a linear dispersion. When supported by the bare Ni(111) surface [Fig. 3(c)], the strong interaction between graphene π bands and the metal d bands destroys the Dirac cone and opens a gap of ≈ 400 meV around the Fermi level. Chemisorption on the metal surface, predicted by DFT-D, leads to a minimum C-Ni distance of 2.11 Å. This is consistent with the experimental reports as well as previous theoretical reports [44–46].

The intercalation of 3/4 ML of Au between the graphene and the Ni(111) surface weakens the graphene-support interaction and decouples the Ni(d) and C(p) electron states. The weaker interaction results from the charge transfer between Au and Ni that saturates the Ni d bands and shifts them to lower energies. In the 3/4 ML Au/Ni(111) system, it is the Au d band that mainly falls at the Fermi level. As a result, the graphene states are weakly perturbed and the overall shape of the Dirac cone is recovered [Fig. 3(d)]. The Dirac point is shifted to nearly 0.35 eV below the Fermi level and a very small band gap of ≈ 20 meV is present. The calculated equilibrium distance between graphene and the Au ML is 3.11 Å, a typical physisorption situation where the interaction is rather weak. This value is very close to the previous reports of 3.27 [47] and 3.31 Å [48] based on DFT studies. Quite interestingly, the precise position of the Dirac point and the band-gap opening turns out to be very sensitive to the graphene-support separation. In our calculation, inclusion of dispersion terms into the Kohn-Sham Hamiltonian with the DFT-D approximation leads to a slight overestimation of the Au-graphene binding, resulting in a negative doping in the graphene plane and a resulting downward shift (-0.35 eV) in the Dirac cone with respect to the Fermi level, as seen in Fig 3(d). This negative doping is, however, consistent with the previous reports on Au-graphene interfaces for such distance [48,49].

To show the variation of doping polarity with respect to the height, we artificially increased the separation between Au and graphene planes to 3.42 and 3.88 Å and plotted the band structure in Figs. 3(e) and 3(f). In Fig. 3(e), the doping is close to zero and, in Fig. 3(f), the doping polarity is already reversed. For a better description of the charge transfer, in Fig. 4 we plot the charge-density difference induced in the graphene/Au/Ni system when the graphene plane is adsorbed onto the Au/Ni substrate. Figures 4(a) and 4(b) show an accumulation of charge (red) at the graphene plane, while Fig. 4(c) shows only depletion (blue), indicating negative and positive doping, respectively.

However, as we shall see later, the effect of negative doping of the graphene due to the proximity of Au atoms is considerably smaller than the effect introduced by doping with alkali adatoms.

C. Energetics and structure of alkali-doped supported graphene

The calculated binding energies of the alkali atoms to graphene supported by the Au/Ni(111) substrate are reported in Table II. As shown in Table II, the alkali atoms prefer to adsorb on the hollow site of the graphene hexagonal
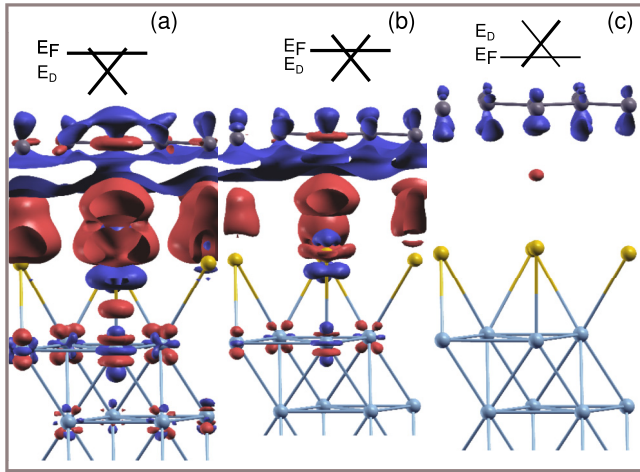
FIG. 4. (Color online) Variation of charge-density difference as a function of graphene-gold distance. Red and blue regions indicate the accumulation and depletions of charge. The doping polarity with respect to the Fermi level is schematically represented at the top of each panel. E_F and E_D represent Fermi level and the Dirac cones, respectively. An isovalue of 0.002 a.u. is used for visualizing the densities.

ring and show similar energetics as in the pristine case (cf. Table I.) Here, we have considered two configurations: (i) adsorbed on top of the graphene plane (denoted as **A** hereafter) and (ii) intercalated between the graphene plane and the Au/Ni(111) substrate (denoted as **I**). Among all the studied configurations, Li displays the largest binding energy for both **I** and **A** configurations, while Na and K display the lowest binding energy for the **A** and **I** configurations, respectively. With respect to adsorption on the freestanding graphene, the substrate increases the binding energy on supported graphene (configuration **A**) by ≈ 0.2 eV. This effect is common to all the alkali atoms (see Tables II and I).

All alkali atoms display an energetic preference to intercalate at the graphene/substrate interface: The adsorption energy in configuration **I** is considerably lower in energy than in **A**. The energy difference between these two configurations ranges from -1.12 to -0.62 eV for Li and K, respectively. In order to explain this thermodynamic preference for alkali-atom intercalation, we have calculated the binding energy of the alkali atoms to a Au(111) surface having its calculated equilibrium lattice parameter of 4.17 Å. A single adatom is adsorbed onto the 2×2 supercell and the system was relaxed

TABLE II. Energetics (in eV) of alkali-functionalized Au/Ni(111) supported graphene. E_{H-T} is the energy difference between the hollow and top sites for the adsorption of the alkali atoms in the graphene plane. **A** and **I** represents the binding energy for adsorption and intercalation, while $\delta(\mathbf{A} - \mathbf{I})$ represents the relative binding-energy difference between adsorption and intercalation.

Alkali	E_{H-T}	**A**	**I**	$\delta(\mathbf{A} - \mathbf{I})$
Li	-0.35	-1.60	-2.72	-1.12
Na	-0.13	-1.17	-2.04	-0.87
K	-0.07	-1.34	-1.96	-0.62
Rb	-0.07	-1.42	-2.11	-0.69

TABLE III. Average height of the alkali-atom layers (in Å) when intercalated **I** and adsorbed **A**. Heights are calculated from the optimized structures by taking the difference in the z coordinates of the layers (see Fig. 1 for definitions of the symbols). X denotes the alkali atom, while Δz indicates the rumpling in the respective atomic layer.

Property	Adsorbed **A**				Intercalated **I**			
	Li	Na	K	Rb	Li	Na	K	Rb
h_{C-Au}	3.10	3.12	3.11	3.10	3.88	4.44	5.43	5.67
h_{X-C}	1.85	2.36	2.76	2.90	1.85	2.33	2.76	2.92
h_{X-Au}	4.95	5.48	5.87	6.00	2.03	2.11	2.67	2.75
h_{Au-Ni}	2.33	2.33	2.32	2.32	2.39	2.55	2.37	2.37
Δz_{C}	0.03	0.02	0.01	0.01	0.02	0.01	0.01	0.01
Δz_{Au}	0.25	0.25	0.25	0.24	0.67	0.87	0.56	0.59
Δz_{Ni}	0.02	0.01	0.02	0.02	0.07	0.06	0.03	0.04

by fixing the bottom two layers to their bulk position. The calculated adsorption energies of Li, Na, K, and Rb are -2.58, -2.38, -2.54, and -2.74 eV, respectively. These values are of the same order of those obtained for the alkali atoms intercalated at the graphene/Au interface that range from -1.96 to -2.76 eV. We therefore conclude that the large driving force for alkali-atom intercalation is governed by the high affinity of Au relative to alkali atoms, which leads to the formation of strongly bound ions at the metal substrate. This conclusion on the ionic state of the dopant will be fully supported by the following analysis of the electronic structure.

We note that experimentally K has been shown to intercalate at the graphene/Au/Ni(111) interface, while Li, Na, and Rb were reported to adsorb on the graphene surface [27]. More recent measurements suggest that the position of the alkali atoms depends on the temperature of the annealing so that the diffusion of the adsorbate from the external surface (configuration **A**) to the intercalated configuration **I** can ultimately be controlled by kinetic effects [50]. On the basis of previous reports, we can say that even for the smallest atom of the series, i.e., Li, a diffusion path through the hexagonal ring has a very high barrier (8 eV for LiC_6 [51]). This suggests that intercalation proceeds at the graphene edges or at grain boundaries. Indeed, a recent paper on the intercalation of alkali atoms in graphite shows an activation energy for the in-plane diffusion of the K atom as low as 0.14 eV for KC_8 [52].

The intercalation of alkali atoms leads to a large increase of the graphene/substrate distance that decouples graphene from the substrate. This will clearly destroy any moiré pattern present due to the lattice mismatch. With respect to the adsorbed configuration **A**, the graphene-substrate distance in the intercalated configuration **I** monotonically increases by 0.77 Å for Li to 2.56 Å for Rb (h_{C-Au}, Table III). A similar trend, which correlates with the ionic size, is also displayed in the distance between the alkali atom X and the Au ML (h_{X-Au}). The formation of a strong X-Au bond pulls out gold atoms from the substrate, thus inducing a rumpling in the Au ML (Δz_{Au}) and deviations from the ideal elevation of the Au ML from the Ni(111) surface (h_{Au-Ni}). Quite differently, the structure of the substrate is weakly affected when the alkali atom adsorbs on the graphene surface (h_{C-Au}, h_{Au-Ni}, and ΔZ_{Au}).
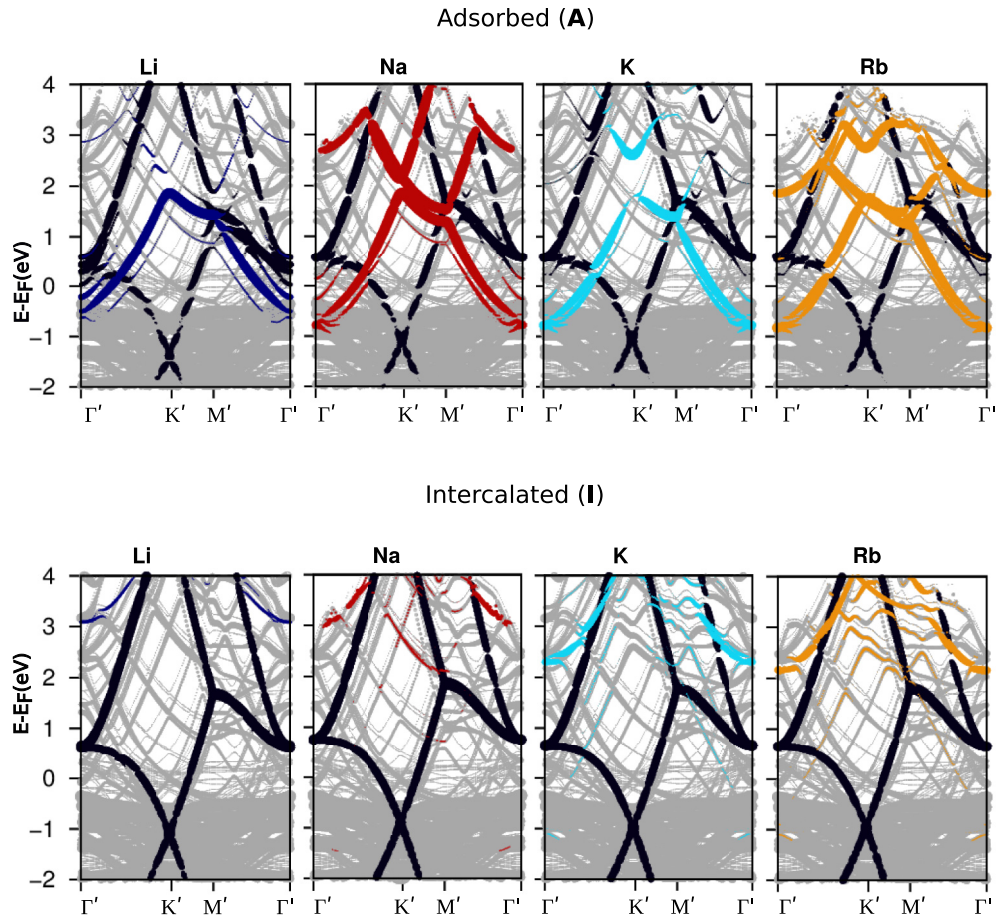
FIG. 5. (Color online) Calculated atom-projected band structure of graphene supported by the Au/Ni surface and functionalized with alkali metals, either adsorbed (top panels) or intercalated (bottom panels). Color code as in Fig. 2.

D. Electronic structure of alkali-doped supported graphene

The effects on the electronic structure induced by alkali doping are displayed and analyzed in Fig. 5, which shows the calculated atom-projected band structure. The black lines correspond to the electronic states with contributions solely from C atoms. They therefore represent the states with a high spatial localization on the graphene layer. It is evident that the overall shape of the graphene band structure is preserved by the functionalization with all of the alkali dopants considered here, independently of the adsorbed or intercalated state. The main effect of the doping is a quasirigid shift of the graphene bands to lower energies. We quantify this shift in Table IV, which reports the energy difference between the Dirac point (E_{DP}) and the Fermi level (E_F) for the freestanding and supported cases (**A** and **I** configurations). Adsorption on supported graphene (configuration **A**) does not significantly perturb the position of the Dirac cone with respect to adsorption on freestanding graphene. The shifts ΔE_{free} and $\Delta E_{\text{supp}}^{\mathbf{A}}$ for Na, K, and Rb agree within 50 meV with respect to the pristine case ranging between -1.01 and -1.07 eV, while Li adsorption yields larger shifts, both in the freestanding (-1.48 eV) and supported (-1.32 eV) cases. However, the deviation from the pristine case is only 160 meV. This close agreement between the adsorption of alkali atoms on pristine graphene as well as the adsorption on the supported case clearly indicates that

the graphene layer is mostly doped by the electrons from the alkali, and the Au atom has little effect on the doping. This can be directly attributed to a much closer separation of the alkali adatom compared to the Au monolayer with respect to the graphene plane. This is further verified by analyzing the band structure (K-doped system) by artificially increasing the Au graphene separation to 3.42 Å, corresponding to nearly zero doping as shown in Fig. 3, and by keeping the graphene-alkali distance the same. The band structure did not show any change in the shift of the Dirac cone. However, we note that upon

TABLE IV. Energy shift in the Dirac point calculated with respect to the Fermi level for pristine (ΔE_{free}, in eV) as well as the supported ΔE_{supp} graphene with adsorbed (**A**) or intercalated (**I**) alkali atoms. E_g indicates the gap in the Dirac cone eventually present in the system.

Alkali (X)	$\Delta E = E_{DP} - E_F$		
	ΔE_{free}	$\Delta E_{\text{supp}}^{\mathbf{A}}$ (E_g)	$\Delta E_{\text{supp}}^{\mathbf{I}}$
Li	-1.48	$-1.32\ (0.05)$	-1.08
Na	-1.06	$-1.06\ (0.05)$	-0.90
K	-1.07	$-1.02\ (0.05)$	-0.98
Rb	-1.05	$-1.01\ (0.05)$	-0.96

adsorption of all alkali atoms on supported graphene, a small gap ($\approx$50 meV; see E_g in Table IV) opens around the graphene Dirac cone at the Fermi level. This gap can easily be assigned to a slight A-B sublattice symmetry breaking in the graphene plane due to the asymmetry in the underlying Au monolayer as in the supported case. On the other hand, the intercalation of the alkali atoms yields a smaller shift of the graphene Dirac cone, ranging from -0.90 to -1.08 eV. In this case, the alkali adatom transfers charge both to the graphene and the substrate, slightly reducing the negative doping in the graphene plane.

The energy shifts of the Dirac cone presented above are obviously correlated to the charge transfer between the alkali adatom and the graphene/substrate. It turns out that this charge transfer is strongly dependent on the actual position of the dopant atoms: The **A** and **I** configurations lead to very different charge states of the alkali atom, but to remarkably similar charge states of the graphene sheet (i.e., similar electron doping). To understand this result, we analyze the band structure projected on the alkali atoms (see color lines in Fig. 5).

When these dopants are adsorbed on the graphene surface (top panels), the resulting 2×2 overlayer has a clear metallic character, with the Fermi level crossing the band formed by the s states of the alkali atoms. This is similar to adsorption on freestanding graphene (see Fig. 2). Also, in this supported case **A**, there is a partial charge transfer from the adatom to graphene that shifts the energy of the Dirac cone to lower energies. Quite importantly, this charge redistribution involves primarily the adatom and the graphene, while the substrate does not participate (see charge-density difference in Fig. 6, top panels).

When the dopants are intercalated between graphene and the metal substrate (bottom panels in Fig. 5), the bands formed by the s states of the alkali atoms are unoccupied, as their energies are more than 2 eV above the Fermi level. In the intercalated configuration, the dopants are therefore fully ionized. Differently from the **A** case, the charge donated by the dopants is in the intercalated case accepted by both the graphene and the support. The analysis of the charge-density difference (Fig. 6, bottom panels) clearly shows the consistent charge buildup between the alkali dopant and the underlying Au atom, thus supporting the formation of the strong X-Au bond discussed in Sec. III C. The comparison of the charge-density differences calculated for the **A** and **I** configurations (top and bottom panels in Fig. 6; same isovalue in all panels) clearly demonstrates that the amount of charge accepted by the graphene sheet is comparable in the adsorbed and intercalated cases. Recently, Fedorov *et al.* [27] reported the shift in the Dirac cone when the alkali atom is adsorbed/intercalated in the Au/Ni(111) supported graphene. They report a shift of 1.17 for K (**I**) and 1.52, 1.22, 1.35 eV, respectively, for Li, Na, and Rb (**A**). Our values are in excellent agreement with these measurements, with a maximum deviation of 0.3 eV. The deviation can be attributed to the coverage and temperature effects.

The Bader charge analysis is consistent with this conclusion. Table V reports the difference in the Bader charge of the adatom X, and of the C, Au, and uppermost Ni layers. When comparing the values for the adsorbed and intercalated configurations, the dopants display a large variation (0.11–0.35e), while the C atoms display more similar values (0.01–0.05e), thus showing that graphene accepts almost the
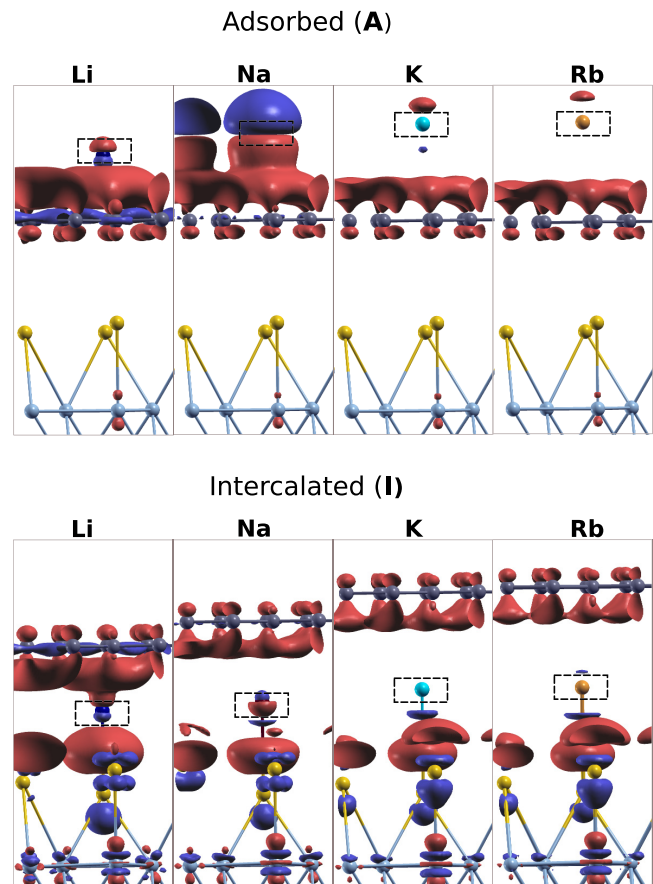
FIG. 6. (Color online) Charge-density difference due to the adsorption/intercalation of alkali atoms (surfaces plotted for isovalue of 0.002 a.u.). Red and blue regions indicate charge accumulation and depletion, respectively. The adatom location is indicated by rectangular boxes.

same charge, independent of the position of the dopant. Conversely, there is a clear increase in the charge of the Au layer in the intercalated configurations. This further demonstrates that the fully ionic state of the intercalated dopant is determined by the metallic substrate and not by the graphene layer.

This result suggests that measuring the shift of the Dirac cone (for example, by photoemission spectroscopy) does not allow one to discriminate between the adsorbed and

TABLE V. Net atomic Bader charge (δ) for the alkali atoms adsorbed (**A**) or intercalated (**I**) in the supported graphene. The charges are calculated with respect to their formal charges. Negative/positive values indicate gain/loss of charge.

Alkali (X)	δX		δC		δAu		δNi (top layer)	
System	**A**	**I**	**A**	**I**	**A**	**I**	**A**	**I**
Li	0.77	0.88	-0.09	-0.04	-0.15	-0.29	0.08	0.06
Na	0.52	0.83	-0.05	-0.03	-0.13	-0.20	0.07	0.08
K	0.44	0.79	-0.04	-0.03	-0.15	-0.27	0.08	0.06
Rb	0.42	0.78	-0.04	-0.03	-0.14	-0.27	0.08	0.06

intercalated configurations of the alkali atoms or to infer their charge state. The commensurate cell used in the present study represents a good reference for the maximum limit of alkali coverage. Any relaxation of the periodicity of the alkali-atom overlayer or island formation would thus reduce the coverage. As a direct consequence, the intensity of the doping will fall and therefore the downshift in the Dirac cone due to charge transfer will be lessened.

IV. CONCLUSIONS

Doping with alkali atoms is a viable strategy to engineer the electronic properties of graphene. We have presented here a systematic computational study of the changes in the atomistic and electronic structures due to adsorption of alkali atoms (Li, Na, K, Rb) to metal-supported graphene. The Au/Ni(111) substrate is taken as a case study because it replicates the electronic properties of freestanding graphene and because of the available experimental data. Our DFT calculations demonstrate that the alkali atoms of our set can chemisorb either on an exposed surface of the supported graphene or intercalated at the graphene/metal interface. The atomistic and electronic band structures show that adsorption with a 2×2 surface periodicity leads to a metallic overlayer, while intercalation leads to ionization of the alkali dopants. The

metallic character plays an important role in the cohesion of the alkali overlayer.

The computed energetics shows that the intercalated configuration is the most stable for all of the dopants. We explain the origins of this preferential segregation with the high affinity of Au relative to the alkali atoms. Alkali intercalation leads to the decoupling of graphene from the metal support. Both surface adsorption and interface intercalation lead to a quasirigid shift of the graphene bands towards lower energies. The shift for supported graphene is always smaller than the corresponding shift for the freestanding graphene. Adsorption leads to a slightly larger shift compared to intercalation: apart from Li, the energy shift of the two configurations is smaller than 160 meV. These data may be useful for interpreting photoemission spectra sampling the valence band. More generally, the present systematic analysis provide useful principles for guiding graphene band structure engineering via alkali-atom doping.

[1] A. Geim and K. Novoselov, Nat. Mater. **6**, 183 (2007).

[2] K. Novoselov, A. Geim, S. Morozov, D. Jiang, M. Katsnelson, I. Grigorieva, S. Dubonos, and A. Firsov, Nature (London) **438**, 197 (2005).

[3] P. A. Khomyakov, G. Giovannetti, P. C. Rusu, G. Brocks, J. van den Brink, and P. J. Kelly, Phys. Rev. B **79**, 195425 (2009).

[4] D. Eom, D. Prezzi, K. T. Rim, H. Zhou, M. Lefenfeld, S. Xiao, C. Nuckolls, M. S. Hybertsen, T. F. Heinz, and G. W. Flynn, Nano Lett. **9**, 2844 (2009).

[5] S. Marchini, S. Günther, and J. Wintterlin, Phys. Rev. B **76**, 075429 (2007).

[6] S.-Y. Kwon, C. V. Ciobanu, V. Petrova, V. B. Shenoy, J. Bareo, V. Gambin, I. Petrov, and S. Kodambaka, Nano Lett. **9**, 3985 (2009).

[7] I. Pletikosic, M. Kralj, P. Pervan, R. Brako, J. Coraux, A. T. N'Diaye, C. Busse, and T. Michely, Phys. Rev. Lett. **102**, 056808 (2009).

[8] P. Sutter, J. T. Sadowski, and E. Sutter, Phys. Rev. B **80**, 245411 (2009).

[9] B. Song, D. Li, W. Qi, M. Elstner, C. Fan, and H. Fang, ChemPhysChem **11**, 585 (2010).

[10] L. Gao, J. R. Guest, and N. P. Guisinger, Nano Lett. **10**, 3512 (2010).

[11] S. Grandthyll, S. Gsell, M. Weinl, M. Schreck, S. Hüfner, and F. Müller, J. Phys.: Condens. Matter **24**, 314204 (2012).

[12] F. Bianchini, L. L. Patera, M. Peressi, C. Africh, and G. Comelli, J. Phys. Chem. Lett. **5**, 467 (2014).

[13] P. Janthon, F. Viñes, S. M. Kozlov, J. Limtrakul, and F. Illas, J. Chem. Phys. **138**, 244701 (2013).

[14] W.-B. Zhang, C. Chen, and P.-Y. Tang, J. Chem. Phys. **141**, 044708 (2014).

[15] A. Varykhalov, J. Sánchez-Barriga, A. M. Shikin, C. Biswas, E. Vescovo, A. Rybkin, D. Marchenko, and O. Rader, Phys. Rev. Lett. **101**, 157601 (2008).

[16] A. Varykhalov, M. R. Scholz, T. K. Kim, and O. Rader, Phys. Rev. B **82**, 121101 (2010).

[17] A. Generalov and Y. Dedkov, Carbon **50**, 183 (2012).

[18] D. Haberer, L. Petaccia, A. V. Fedorov, C. S. Praveen, S. Fabris, S. Piccinin, O. Vilkov, D. V. Vyalikh, A. Preobrajenski, N. I. Verbitskiy, H. Shiozawa, J. Fink, M. Knupfer, B. Büchner, and A. Grüneis, Phys. Rev. B **88**, 081401 (2013).

[19] G. Profeta, M. Calandra, and F. Mauri, Nat. Phys. **8**, 131 (2012).

[20] T. E. Weller, M. Ellerby, S. S. Saxena, R. P. Smith, and N. T. Skipper, Nat. Phys. **1**, 39 (2005).

[21] M. Calandra and F. Mauri, Phys. Status Solidi B **243**, 3458 (2006).

[22] I. I. Mazin, Phys. Rev. Lett. **95**, 227001 (2005).

[23] S. Chakravarty and S. Kivelson, Europhys. Lett. **16**, 751 (1991).

[24] S. Chakravarty, M. P. Gelfand, and S. Kivelson, Science **254**, 970 (1991).

[25] Z. K. Tang, L. Zhang, N. Wang, X. X. Zhang, G. H. Wen, G. D. Li, J. N. Wang, C. T. Chan, and P. Sheng, Science **292**, 2462 (2001).

[26] M. Kociak, A. Y. Kasumov, S. Guéron, B. Reulet, I. I. Khodos, Y. B. Gorbatov, V. T. Volkov, L. Vaccarini, and H. Bouchiat, Phys. Rev. Lett. **86**, 2416 (2001).

[27] A. V. Fedorov, N. I. Verbitskiy, D. Haberer, C. Struzzi, L. Petaccia, and A. Grneis, Nat. Commun. **5**, 3257 (2014).

[28] J. P. Perdew, K. Burke, and M. Ernzerhof, Phys. Rev. Lett. **77**, 3865 (1996).

[29] S. Grimme, J. Comput. Chem. **27**, 1787 (2006).

[30] P. Giannozzi, S. Baroni, N. Bonini, M. Calandra, R. Car, C. Cavazzoni, D. Ceresoli, G. L. Chiarotti, M. Cococcioni, I. Dabo, A. Dal Corso, S. de Gironcoli, S. Fabris, G. Fratesi, R. Gebauer, U. Gerstmann, C. Gougoussis, A. Kokalj, M. Lazzeri, L. Martin-Samos, N. Marzari, F. Mauri, R. Mazzarello, S. Paolini, A. Pasquarello, L. Paulatto, C. Sbraccia, S. Scandolo, G. Sclauzero, A. P. Seitsonen, A. Smogunov, P. Umari, and R. M. Wentzcovitch, J. Phys.: Condens. Matter **21**, 395502 (2009).

[31] M. H. Kang, S. C. Jung, and J. W. Park, Phys. Rev. B **82**, 085409 (2010).

[32] L. Qiao, C. Qu, H. Zhang, S. Yu, X. Hu, X. Zhang, D. Bi, Q. Jiang, and W. Zheng, Diam. Relat. Mater. **19**, 1377 (2010).

[33] X. Liu, C. Z. Wang, M. Hupalo, W. C. Lu, M. C. Tringides, Y. X. Yao, and K. M. Ho, Phys. Chem. Chem. Phys. **14**, 9157 (2012).

[34] K.-H. Jin, S.-M. Choi, and S.-H. Jhi, Phys. Rev. B **82**, 033414 (2010).

[35] M. Fuentes-Cabrera, M. I. Baskes, A. V. Melechko, and M. L. Simpson, Phys. Rev. B **77**, 035405 (2008).

[36] K. T. Chan, J. B. Neaton, and M. L. Cohen, Phys. Rev. B **77**, 235430 (2008).

[37] W. Tang, E. Sanville, and G. Henkelman, J. Phys.: Condens. Matter **21**, 084204 (2009).

[38] S. M. Kozlov, F. Vies, and A. Grling, J. Phys. Chem. C **116**, 7360 (2012).

[39] W. Zhao, S. M. Kozlov, O. Hofert, K. Gotterbarm, M. P. A. Lorenz, F. Vines, C. Papp, A. Gorling, and H.-P. Steinruck, J. Phys. Chem. Lett. **2**, 759 (2011).

[40] M. Vanin, J. J. Mortensen, A. K. Kelkkanen, J. M. Garcia-Lastra, K. S. Thygesen, and K. W. Jacobsen, Phys. Rev. B **81**, 081408(R) (2010).

[41] M. Dion, H. Rydberg, E. Schröder, D. C. Langreth, and B. I. Lundqvist, Phys. Rev. Lett. **92**, 246401 (2004).

[42] K. Lee, E. D. Murray, L. Kong, B. I. Lundqvist, and D. C. Langreth, Phys. Rev. B **82**, 081101 (2010).

[43] J. P. P. Ramalho, J. R. B. Gomes, and F. Illas, R. Soc. Chem. Adv. **3**, 13085 (2013).

[44] Y. Gamo, A. Nagashima, M. Wakabayashi, M. Terai, and C. Oshima, Surf. Sci. **374**, 61 (1997).

[45] D. E. Parreiras, E. A. Soares, G. J. P. Abreu, T. E. P. Bueno, W. P. Fernandes, V. E. de Carvalho, S. S. Carara, H. Chacham, and R. Paniago, Phys. Rev. B **90**, 155454 (2014).

[46] E. Voloshina and Y. Dedkov, Phys. Chem. Chem. Phys. **14**, 13502 (2012).

[47] C. Gong, G. Lee, B. Shan, E. M. Vogel, R. M. Wallace, and K. Cho, J. Appl. Phys. **108**, 123711 (2010).

[48] G. Giovannetti, P. A. Khomyakov, G. Brocks, V. M. Karpan, J. van den Brink, and P. J. Kelly, Phys. Rev. Lett. **101**, 026803 (2008).

[49] J. Sławińska, P. Dabrowski, and I. Zasada, Phys. Rev. B **83**, 245429 (2011).

[50] L. Petaccia *et al.* (unpublished).

[51] S. Thinius, M. M. Islam, P. Heitjans, and T. Bredow, J. Phys. Chem. C **118**, 2273 (2014).

[52] Z. Wang, A. P. Ratvik, T. Grande, and S. M. Selbach, R. Soc. Chem. Adv. **5**, 15985 (2015).